NEW MEXICO TECH
SCIENCE' ENGINEERING. RESEARCH UNIVERSITY

To Prof. Frank Huang (Chair) and the HD&A Committee,

For consideration of the Langmuir award, I wish to nominate Mr. Daniel Leonard, M.S. in Chemistry, for his 2015 publication in the journal: *ACS Applied Materials & Interfaces*.

Of the many graduate students I've advised, Mr. Leonard has made perhaps the most challenging changes in his career direction to achieve a first author publication in this high impact journal. Dan's B.S. degree from UC Davis was in Enology and Viticulture (the science of growing grapes and making wine). After several years of working in California wineries, Dan made a significant change in career direction by choosing the path toward an advanced degree in chemistry. So, prior to NMT, he completed his post-baccalaureate studies at UC Riverside thereby completing a year of Physical Chemistry and demonstrating proficiency for acceptance to graduate studies at NMT Chemistry.

The publication (attached below): "Photocatalyzed Reduction of Bicarbonate to Formate: Effect of ZnS Crystal Structure and Positive Hole Scavenger" was ranked among the top 20% by the reviewers in their acceptance decision. The paper brought three very important findings to light in the area of photo-driven reduction of CO2 (and bicarbonate the predominant hydrated form in neutral water).

(1) After 20 years since the first report of non-toxic, earth-abundant, ZnS catalyzing CO2 to formate, no one had considered comparing the two crystal structures of ZnS (sphalerite vs wurtzite) and their catalytic activity. Dan found wurtzite to be considerably better and was able to account for this improved yield based on differences in catalytic surface area between the two crystal forms.

(2) In addition, since the first ZnS photo reduction study published in 1994 involving micro-size catalysts, no researchers had considered making the step toward nano particulate ZnS. Dan synthesized both wurtzite andsphalerite NPs of ZnS and found that per mass comparisons, nano particulate particles were far more effective catalysts.

(3) Finally, much of these previous studies utilized a fossil fuel derived "hole scavenger" to maintain the photo reduction cycle such as 2-propanolgetting oxidized to acetone. Dan found that glycerol, a by-product in the biodiesel B-100 process, gave 12x more formate production than 2-propanol. So, a renewable "green chemistry" co-solvent, along with water, has been shown to be an effective replacement.

In closing, the 2015 impact factor for *ACS Applied Materials & Interfaces* is 6.75. Overall, the work offers a significant contribution to the field of CO2 utilization, which is economically preferred to the alternative CO2 sequestration. Dan is now pursuing his Chemistry Ph.D. at Oregon State U.

Thanks for considering this nomination,

Michael D Heagy

Michael Heagy
Professor of Chemistry

Chemistry Department, Jones Hall 575-835-5263

801 Leroy Place • Socorro • New Mexico • 87801 • http://infohost.nmt.edu/~chem/___

ACS APPLIED MATERIALS & INTERFACES

Research Article

www.acsami.org

Photocatalyzed Reduction of Bicarbonate to Formate: Effect of ZnS Crystal Structure and Positive Hole Scavenger

Daniel P. Leonard, Hanqing Pan, and Michael D. Heagy*

New Mexico Institute of Mining & Technology, Socorro, New Mexico 87801, United States

Supporting Information

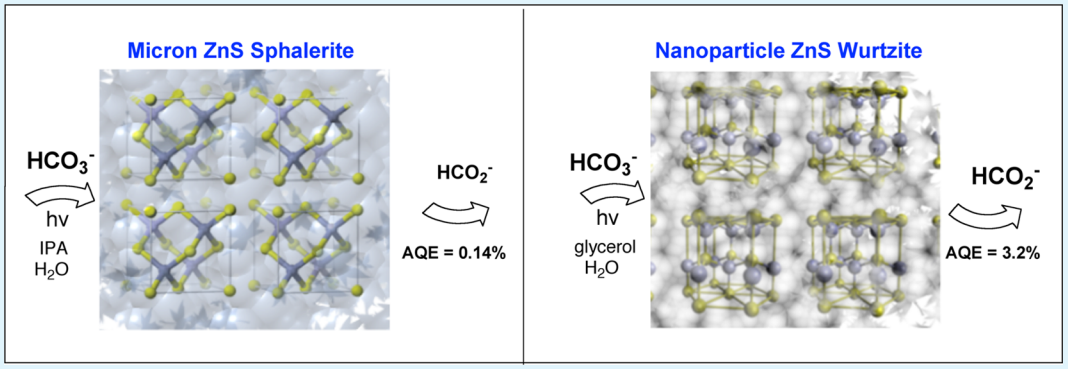

ABSTRACT: Zinc sulfide is a promising catalyst due to its abundance, low cost, low toxicity and conduction band position that enables the photoreduction of CO_2 to formic acid. This study is the first to examine experimentally the photocatalytic differences between wurtzite and sphalerite under the parameters of size (micrometer and nanoscale), crystal lattice, surface area, and band gap on productivity in the photoreduction of HCO_3^-. These photochemical experiments were conducted under air mass coefficient zero (AM 0) and AM 1.5 solar simulation conditions. We observed little to no formate production under AM 1.5, but found linear formate production as a function of time using AM 0 conditions. Compared to earlier reports involving bubbled CO_2 in the presence of bicarbonate, our results point to bicarbonate as the species undergoing reduction. Also investigated are the effects of three hydroxylic positive hole scavengers, ethylene glycol, propan-2-ol (isopropyl alcohol, IPA) and glycerol on the reduction of HCO_3^-. Glycerol, a green solvent derived from vegetable oil, greatly improved the apparent quantum efficiency of the photocatalytic reduction.

KEYWORDS: *carbon dioxide, bicarbonate photoreduction, formate, ZnS nanoparticles, wurtzite, sphalerite*

INTRODUCTION

There is growing interest in the development of new technologies for sustainable energy production such as photocatalyzed reduction of carbon dioxide and sunlight. One possible avenue to achieve this goal is the replacement of existing fossil carbon infrastructure with one based on the synthesis of methanol. A key tenet and technological challenge of "the methanol economy" is solar-driven conversion of carbon dioxide to formic acid and ultimately methanol.[1] Efforts toward photoreduction of CO_2 and its aqueous forms of carbonic acid, bicarbonate and carbonate (eq 1) hold the promise of greenhouse gas mitigation by mimicking natural photosynthesis via energy storage in chemical bonds.[2,3]

$$H_2O + CO_2 \rightleftharpoons HCO_3^- + H^+ \rightleftharpoons CO_3^{2-} + 2H^+ \quad (1)$$

Because the energy density of hydrocarbons vastly outstrips that of other potential fuels, the simplest class, C1 fuels are highly attractive as synthetic targets. Methanol, for example, contains roughly twice the amount of energy per unit volume than hydrogen gas compressed to 700 psi.[4] Similarly, formic acid, another C1 fuel, is roughly equivalent in energy density to compressed hydrogen. To that end, the photocatalytic transformation of CO_2 into fuels has attracted considerable attention as a potentially sustainable technology.[5−10] Photochemical catalysts for CO_2 reduction can be divided into two main categories: metal complexes, primarily ruthenium mono-(bipyridyl) and bis(bipyridyl) dicarbonyl complexes, and semiconductor materials such as TiO_2, CdS or ZnS.[11] Both forms of photocatalysts in the presence of propan-2-ol have mostly resulted in formate production relative to CO production. According to a recent comprehensive review of semiconductor photocatalysts, we found it interesting that the last report involving ZnS utilized micrometer sized particles and was authored by Yoneyama; one of the foremost pioneers along with Inoue in photochemical CO_2 reduction.[12,13] Despite the importance of ZnS in these early photochemical conversions, no comparative investigation into the photocatalytic behavior of the two ZnS crystal forms (cubic vs hexagonal) has been

Received: July 8, 2015
Accepted: October 15, 2015
Published: October 15, 2015

DOI: 10.1021/acsami.5b06054
ACS Appl. Mater. Interfaces 2015, 7, 24543−24549

reported. Therefore, we carried out an investigation into the nanoparticulate size regime including the effects of surface area on productivity and disclose key differences between the two ZnS crystal forms. In addition, the efficiencies of these processes have been shown to largely depend on the type of hole-removing agent. Among three different alcohols utilized for this purpose, we demonstrate improved yields of formate using a green chemistry solvent.

The reduction of bicarbonate to formate requires a sacrificial agent to serve as a source of electrons and hydrogen, schematic in Figure 1. When propan-2-ol (isopropyl alcohol, IPA) is used

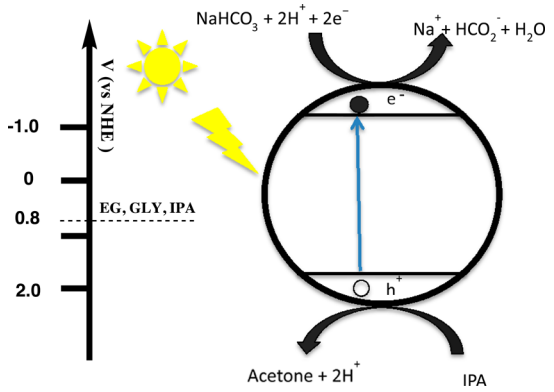

Figure 1. Schematic of representative photoreduction of HCO_3^- to formic acid on ZnS using IPA as a hole scavenger.

as a positive hole scavenger, the oxidation takes place at the hydroxyl carbon, yielding acetone as a byproduct. Prior studies have used a variety of different compounds such as Na_2SO_3, IPA, H_2, H_2S, and 2,5-dihyrofuran (DHF).[14−17] Comparisons between IPA and DHF have demonstrated an increase in formate production with DHF suggesting that the selection of the proper hole scavenger could have a significant effect on the efficiency of this reaction.[18] The use of glycerol has not yet been reported in conjunction with ZnS, whereas in the case of TiO_2, the role of the hole scavenger is thought to be minimal. Glycerol contains one secondary and two primary alcohol groups; all of which are potential sites for oxidation that could enhance the rate of product formation. As shown in Figure 1, the redox potentials of the three electron-donor solvents are centered near 0.8 V (ethylene glycol 0.76 V, IPA 0.80 V and glycerol 0.79 V).[19] Given the proximity of their electrochemical potentials, we hypothesized that differences in formate production rates would be largely due to kinetic properties.

Among the positive hole scavengers compared in this study, ethylene glycol and propan-2-ol, are derived from petroleum sources. Glycerol, on the other hand, is of interest because it can be synthesized biologically, is low cost, environmentally benign and relatively abundant. The production of glycerol is expected to outpace its demand by a factor of 6 by the year 2020.[20] As such, glycerol could serve as a "green" replacement for other petroleum-derived hole scavengers.

EXPERIMENTAL SECTION

Wurtzite Nanoparticle Synthesis (nP-Wurtz). Wurtzite nanoparticles were synthesized via aqueous precipitation.[21] Reagents used were purchased from Fischer Scientific and included Acros Organics $Na_2S{\cdot}9H_2O$, Acros Organics $ZnCl_2$ technical grade 97%. Solutions of $ZnCl_2$ and Na_2S were both prepared with concentrations of 0.1M. The Na_2S solution was added dropwise, over 17 min, to $ZnCl_2$ solution while under vigorous agitation. As soon as the total volume of Na_2S had been added, the resulting colloid was divided into 50 mL aliquots and centrifuged at 2000 rpm and 4 °C for 5 min. The supernatant was discarded, and the pellets were suspended in 40 mL of Milli-Q water, using an ultrasonic bath, and centrifuged. The resulting supernatant was discarded, and the pellets were suspended in 40 mL of 2-propanol (IPA) and then centrifuged. This IPA wash was repeated twice.

Following the final wash, the pellets were again suspended in 10 mL of IPA and combined into a round-bottomed flask. The remaining solvent was removed by vacuum distillation and the remaining powder was placed in the drying oven overnight at 75 °C.

Sphalerite Nanoparticle Synthesis (nP-Sphal). 2.00 g of Merck Reagent ZnO was added to 40 mL of 2 M Na_2S solution (Acros Organics $Na_2S{\cdot}9H_2O$).[22] The mixture was placed in an ultrasonic bath for 30 min. The resulting colloid was then purged with nitrogen gas and transferred to an oil bath of 90 °C, and stirred for 2 h using a magnetic stir bar. The colloid was then cooled to room temperature and washed three times with Milli-Q water and centrifuged at 2000 rpm and 4 °C for 5 min. Following the final water wash, the pellet was washed in IPA, centrifuged and again suspended in IPA before being placed in the drying oven overnight. Larger sphalerite microparticles were purchased from Sigma-Aldrich (ZnS 99.99%, mP-Sphal).

Particle Characterization: Size, Crystal Structure and Surface Area Determination. Hydrodynamic size distributions of the different syntheses were obtained using dynamic light scattering (DLS). Zinc sulfide colloidal suspensions were prepared 1 mg/mL in IPA. The suspensions were scanned using a Microtrac Zetatrac nanoparticle analyzer, and the resulting distributions are shown in Figure S1. Crystal structure information was obtained using an X'Pert Pro X-ray diffraction (XRD) instrument; spectra for nP-Wurtz, nP-Sphal and mP-Sphal are shown in the Supporting Information Figure S2. Surface area measurements were carried out using a Micrometrics ASAP2020 surface area and porosity instrument. Additionally, TEM and HR-TEM were carried out on each of the synthesized particle samples. The mP-Sphal samples purchased from Sigma-Aldrich were too large for quality images to be obtained.

Diffuse Reflectance Spectroscopy (DRS). The dry ZnS particle powders were analyzed using diffuse reflectance spectroscopy in order to estimate the band gap of each ZnS sample. Small amounts of the powders were placed on barium sulfate plates and placed in a Hitachi U-4100 UV−vis spectrophotometer with integration sphere. Wavelengths scanned were from 600 to 240 nm. The resulting reflectance data were converted to absorbance and treated to a Kubelka−Munk function plotted against the energy of the incident light to obtain band energies.[23]

Cyclic Voltammetry. To place the band gaps obtained via DRS on an absolute energy scale, cyclic voltammetry (CV) was required. The procedure for CV was adapted from Fang et al.[24] Suspensions of 0.4 mg/mL of mP-Sphal, 0.2 mg/mL nP-Sphal and 0.25 mg.mL nP-Wurtz were prepared in ethanol. These solutions were sonicated for 1 h in order to ensure suspension. After sonication, 600 μL of 5% Nafion solution was added to the suspension, and 4.5 μL of the resulting solution was pipetted onto polished glassy carbon electrodes (GCE) and allowed to dry. Several applications of the solution were required to ensure full coverage of the GCE surface.

The position of the conduction band minimum (CBM) was obtained using a Solartron Analytical 1470E CellTest system with a standard three-electrode setup: GCE working electrode, saturated Ag/AgCl reference electrode and platinum counter electrode. The electrolyte used was 2 M phosphate buffered water at pH 7. The voltage was swept from −900 to +600 mV at a rate of 100 mV/s.

Photoexperiments and Analysis. *Matrix Preparation.* Reagents used for the preparation of the solutions were Riedel-de Haën $NaHCO_3$ 99.0%, J.T. Baker K_2HPO_4, ACS reagent grade isopropyl alcohol, ethylene glycol and MP Biomedicals highly purified glycerol. The buffer reported by Yoneyama et al. was prepared by dissolving 2.52 g of $NaHCO_3$, 8.71 g of K_2HPO_4 and 7.65 mL of IPA in Milli-Q H_2O giving a final concentration of 0.3 M $NaHCO_3$, 0.5 M K_2HPO_4 and 1 M IPA.[12] When used in photoreduction experiments, high purity CO_2 gas was bubbled through the solution for 30 min. After the putative buffer system proved unsuccessful, a new reaction matrix was

DOI: 10.1021/acsami.5b06054
ACS Appl. Mater. Interfaces 2015, 7, 24543−24549

designed. The new reaction matrix was prepared by dissolving 2.52 g of $NaHCO_3$ and 15.3 mL of IPA in Milli-Q H_2O giving a final concentration of 0.3 and 2 M, respectively. The CO_2 bubbling step was no longer used. For the experiments requiring glycerol or ethylene glycol as the positive hole scavenger, the $NaHCO_3$ concentration remained the same except the 2 M IPA was replaced by 2 M glycerol and ethylene glycol, respectively.

Formic Acid Analysis. For samples utilizing IPA as the hole scavenger, quantification of formic acid was carried out using ion chromatography, Metrohm 720 Personal IC, 9 mM Na_2CO_3 eluent, flow rate 1.0 mL/min, on a Dionex IonPak AS9-HC column and suppressor column with 20 mM H_2SO_4 as a regenerant. A standard curve was prepared using six formic acid standards: 5, 10, 25, 50, 100 and 150 ppm, Supporting Information.

For samples utilizing glycerol as the hole scavenger, the quantification of formic acid required a different IC instrument and setup. The Dionex AS50 IC was equipped with a Dionex CD25 conductivity detector, a Dionex IonPac ICE-AS6 column and a Thermo Scientific AMMS-ICE 300 suppressor column. The reagents used were 0.4 mM heptafluorobutyric acid as the eluent with a flow rate of 1.2 mL/min, and 5 mM tertabutylammonium hydroxide as the regenerant. A standard curve was prepared using 0, 5, 10, 25, 50 and 100 ppm standards, Supporting Information.

Photoexperiments. Experiments for the production of formic acid were carried out in a ScienceTech solar simulator with an AM 0 and AM 1.5 filter. The light source used was a 1000 W xenon arc lamp. The output at sample surface was 100 W/m^2. The particle concentrations were standardized by the average surface area with the resulting concentration of 0.2 mg/mL nP-Wurtz, 1 mg/mL nP-Sphal and 3.4 mg/mL mP-Sphal. The particles were suspended in 10 mL of the matrix described previously by sonication for 30 min.

The suspensions were transferred to quartz test tubes, sealed and placed in the solar simulator. Aliquots of 1.6 mL were taken at 0, 2, 4, 6 and 8 h time points. The samples were centrifuged at 16000 RCF for 2 min to remove the ZnS particles; the resulting supernatant was analyzed using IC.

Apparent Quantum Efficiency. Using an Ophir Photonics Nova II laser energy meter with a Ophir Photonics thermal power sensor attached, the energy output of the solar simulator was measured. This power measurement was converted to moles of photons per second. This photon flux was then used to calculate the apparent quantum efficiency (AQE) of the catalyst using eqs 2 and 3.[25]

$$\text{n mol photons} \cdot \frac{1 \text{ mol } e^-}{\text{mol photons}} \cdot \frac{\text{mol formate}}{2 \text{ mol } e^-} = \text{theoretical} \quad (2)$$

$$\frac{\text{actual mol formate}}{\text{theoretical mol formate}} \cdot 100 = \%\text{AQE} \quad (3)$$

RESULTS AND DISCUSSION

XRD spectroscopy confirmed the selective synthesis of sphalerite and wurtzite crystal forms, and DLS revealed the hydrodynamic particles size distributions to be polydisperse; plots are available in the Supporting Information. The lack of uniformity in particle size is most likely the result of poor control over aggregation during the crystal isolation process. TEM and HR-TEM revealed that although the particles themselves seemed large when characterized by DLS, the large particles are actually aggregates of much smaller crystallites, Figure 2. As noted by Quigg et al., though nanoparticles produced during the synthesis process may be monodisperse in size, they would be unlikely to remain so once suspended in aqueous solution and subjected to the photo-experiment conditions.[26] Aggregation of the nanoparticles was visually evident during the photoexperiments. The size of individual crystals within the aggregates in the case of the nP-Wurtz particles was below the 10 nm threshold that could have

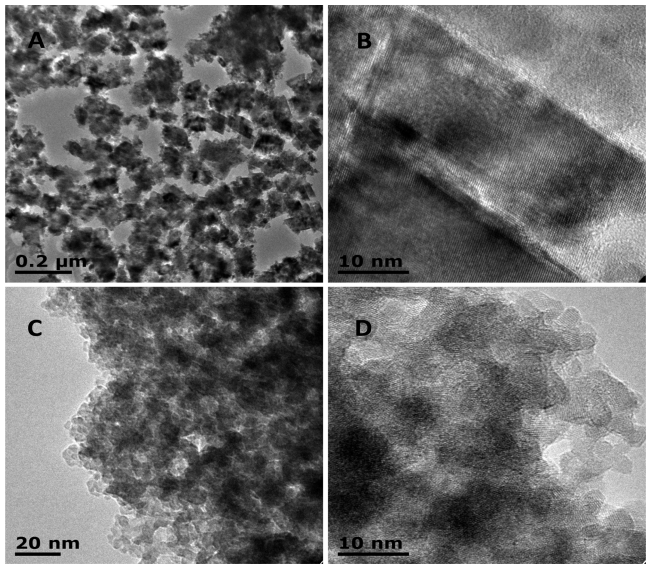

Figure 2. TEM and HR-TEM images of nP-Sphal (A, B) and nP-Wurtz (C, D).

resulted in an increased band gap; however, such an enhancement was not observed.[27]

Large differences in surface area were observed between the nP-Wurtz, nP-Sphal and mP-Sphal populations, Table 1. The

Table 1. Summary of ZnS Characterization Including Crystal Type, Size by DLS, BET Surface Area and AQEs

particle population	crystal type	diameter (nm)	surface area (m^2/g)	AQE in IPA (%)	AQE in EG (%)	AQE in glycerol (%)
mP-Sphal	cubic	934	15.9	0.14	0.49	1.27
nP-Sphal	cubic	173	45.9	0.18	1.39	2.72
nP-Wurtz	hexagonal	83	223	0.90	2.82	3.20
TiO_2	rutile/ anatase 3:1	P-25[29]		0.01		

nP-Wurtz samples possessed a nearly five-fold greater surface area than the nP-Sphal particles. Standardizing the surface area of the catalyst used (based on the mass) compensated for the inherent differences.

To obtain the band gap data, DRS was used. The reflectance plots and resulting Kubelka–Munk plots can be seen in Figure 3. According to the literature, values for the band gap of ZnS range between 3.68 and 3.87 eV.[28] In this case, the particles with the largest band gap are the nP-Sphal at 3.56 eV, whereas the nP-Wurtz and mP-Sphal samples showed equivalent band gaps of 3.37 and 3.36 eV, respectively. The literature values for the band gap of ZnS were obtained using electroluminescence rather than cyclic voltammetry. This likely explains the difference between the reported values and those obtained in our investigation.

With the band gap data in hand via DRS, it was necessary to characterize further the particles by placing these band gaps on an absolute NHE scale using CV; these plots are located in Figure S3 of the Supporting Information. Working in aqueous solution, the conduction band minimum (CBM) was obtained and then combined with the band gap to calculate the position of the valence band maximum (VBM). CV showed the CBM, under our conditions, to reside at −0.45, −0.43 and −0.39 V

DOI: 10.1021/acsami.5b06054
ACS Appl. Mater. Interfaces 2015, 7, 24543−24549

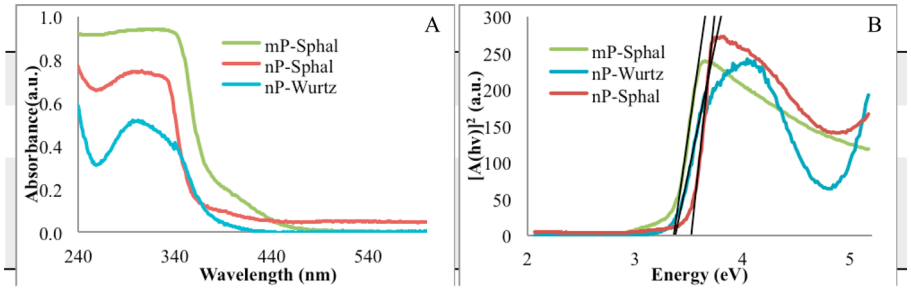

Figure 3. (A) Plots of absorbance. (B) Kubelka–Munk plots revealing the band gaps of the ZnS particle populations.

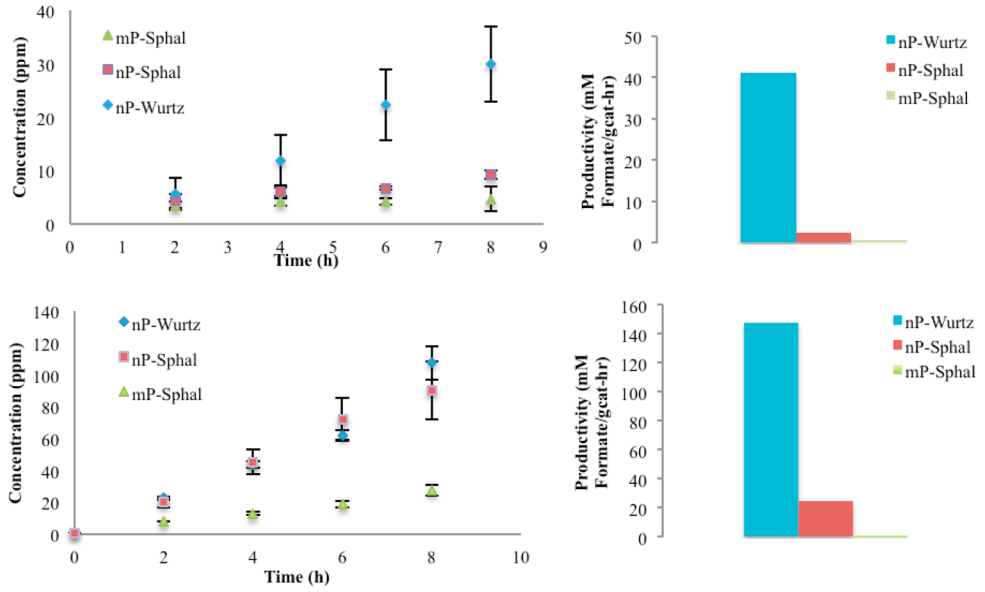

Figure 4. Time course of formate production and specific productivity using the hole scavenger isopropyl alcohol (top graphs) and the hole scavenger glycerol (bottom graphs).

(vs Ag/AgCl sat.) for the nP-Wurtz, nP-Sphal and mP-Sphal samples, respectively. Given the proximity of the two CBMs to each other, the position of the CBM is unlikely to be responsible for observable differences in catalytic productivity of the catalysts.

With the particle populations fully characterized, photoexperiments subsequently could be conducted. While performing photoexperiments with dissolved CO_2, the question of which species is undergoing reduction became an important concern. Previous studies have examined the reduction of CO_2, or bicarbonate, without addressing the pH-dependent equilibrium associated with the hydration of CO_2.[30−33] This led to questions about how the photoexperiments may be affected by changes in pH, which has a profound influence on the substrates available to the catalyst.

Initially, CO_2 gas was bubbled through the matrix for 1 h prior to placing the sample in the solar simulator following the procedure outlined by Yoneyama et al.[13] The pH of this solution was 6.5. At this acidic pH, the relative concentration of $CO_{2(aq)}$ and HCO_3^- is roughly equivalent,[34] and no formate production was observed. When the CO_2 bubbling step was removed, the pH of the matrix solution equilibrated at 8.5. At this pH, the equilibrium significantly favors HCO_3^- over the other C(+IV) species and formate production was observed. To probe further the CO_2 vs HCO_3^- substrate question, a matrix was prepared that replaced the $NaHCO_3$ with Na_2CO_3. This solution equilibrated with the pH of 12.4. At this highly basic pH, the only C(+IV) species with a significant concentration is CO_3^{2-}, and under these conditions no formate production was observed. The only condition leading to detectable levels of formate production was at pH 8.5, at which HCO_3^- is the dominant C(+IV) species. This finding suggests that the preferred substrate for reduction when using ZnS is bicarbonate. Control experiments were conducted in the absence of ZnS, or $NaHCO_3$, when using either IPA or glycerol. None of these conditions resulted in detectable formate.

Ideally, air mass coefficient 1.5 (AM 1.5) solar simulation irradiation would catalyze the reduction of bicarbonate; however, given the band gap of ZnS along with AM 1.5 filtering of wavelengths between 300 and 400 nm, little to no photoreduction products were observed. Under AM 0 solar simulation conditions, the catalysts showed linear production of formate during the 8 h exposure time. Dramatic differences in formate production were observed when comparing nP-Wurtz, nP-Sphal and mP-Sphal crystal populations. Using IPA as the hole scavenger, the nP-Wurtz particles (Figure 4) show superior formate production over the other populations, Despite the compensation in catalyst loading due to surface area differences, our observations show that the nP-Wurtz samples were between 6 and 10 times more productive than the nP-Sphal and mP-Sphal samples. The nP-Sphal and mP-Sphal samples displayed similar AQE values of 0.18% and 0.14%,

DOI: 10.1021/acsami.5b06054
ACS Appl. Mater. Interfaces 2015, 7, 24543−24549

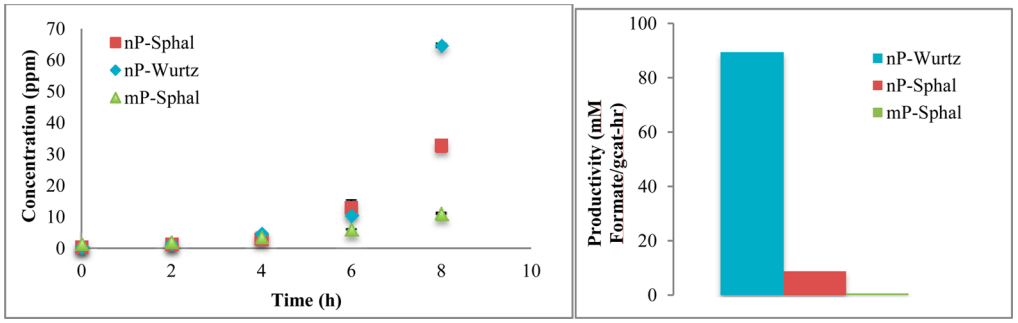

Figure 5. Time course of formate production and specific productivity using ethylene glycol as the positive hole scavenger.

respectively. The nP-Wurtz samples on the other hand displayed a much-improved AQE value of 0.90%.

Catalytic differences between crystalline isoforms have been documented previously between anatase and rutile TiO_2.[35−37] In addition, two studies by Hong et al. examined differences between ZnS isoforms in photocatalytic reactions. In the first study, sphalerite was found to possess a photocatalytic advantage in the degradation of eosin B, an organic pollutant analog.[38] The second study, however, demonstrated that wurtzite possessed greater H_2 production in photocatalytic experiments as well higher photodegradation rates for eosin B when exposed to ambient H_2S.[39] These authors, as well as a similar study by Wang et al., argue that a polarization between Zn-terminated surfaces and S-terminated surfaces is present. This polarization enhances electron/hole separation within wurtzite planes and enables higher rates of catalysis.[40]

When glycerol was used instead of IPA as the electron donor, all of the particle samples showed a dramatic increase in productivity. In fact, the nP-Wurtz and nP-Sphal samples produced roughly equivalent levels of formate over the 8 h exposure time. The mP-Sphal samples also demonstrated a significant boost in productivity, but as shown in Figure 4, not to the same degree as the samples involving nSphal. The AQEs of the particle samples were also dramatically enhanced, increasing to 1.27%, 2.27% and 3.20% for the mP-Sphal, nP-Sphal and nP-Wurtz, respectively. In the case of the nP-Sphal particles, the AQE rose by a factor of 12. Such productivity enhancement is highly promising because glycerol is widely available and can be derived from nonfossil sources. Dimitijevic et al. pointed out in their study that glycerol showed the highest rate of reaction with surface trapped holes.[18] This is due to the abundance of hydroxyl groups on glycerol, which facilitates adsorption onto the particle surface. However, they also concluded that the positive hole scavenger had no effect on efficiency of the CO_2 reduction process. Our results stand in contrast to this conclusion and the intermediate production levels of formate via ethylene glycol (Figure 5) lend support to our hypothesis that increasing the number of primary OH groups leads to improved C−H hole-scavenging reactivity.

Moreover, Valentin et al., in their computational study of surface organic adsorbates, found glycerol to be the best candidate among the organic compounds investigated for use as a positive hole scavenger.[41] Foremost, this experimental work confirms that glycerol is a superior sacrificial hole scavenger under the described photochemical conditions. The sizable boost in productivity observed for the nP-Sphal samples is additional evidence that the surface chemistry at specific crystal facets plays a large role in the activity of the catalysts.

Reports dealing with the mechanism of photocatalytic reduction of CO_2 in carbon-dioxide-saturated aqueous solutions describe the UV irradiation of TiO_2 catalysts.[29] Electron spin resonance (ESR) measurements have detected intermediates such as C· radicals and Ti^{3+} in the excited state complex $(Ti^{3+}-O-)^*$. More recently, a similar complex was reported for zinc oxide in the form of $(Zn^{3+}-O)^*$ upon UV excitation with graphene oxide.[42] On the basis of the chemical similarities between ZnO and ZnS, as well as our control experiments involving bicarbonate and CO_2 saturated solutions, we propose the following redox mechanism (Scheme 1) that

Scheme 1. Proposed Mechanism for the Conversion of Bicarbonate to Formate

Illumination;

$$ZnS \xrightarrow{h\nu} e^-(Zn^{3+}) + h^+$$

$$(Zn^{4+}\text{-}S^{2-}) \xrightarrow{h\nu} (Zn^{3+}\text{-}S^-)^*$$

Oxidation;

$$(CH_3)_2CHOH \xrightarrow[(Zn^{3+}\text{-}S^-)^*]{h^+} 2H^+ + (CH_3)_2CO$$

Reduction;

$$HCO_3^- \xrightarrow[(Zn^{3+}\text{-}S^-)^*]{e^-} \dot{H}CO_3^{2-}$$

$$\dot{H}CO_3^{2-} \xrightarrow[(Zn^{3+}\text{-}S^-)^*]{2H^+ + e^-} HCO_2^- + H_2O$$

invokes $(Zn^{3+}-S)^*$ as the photoexcited semiconductor and takes bicarbonate into account as the substrate undergoing reduction. A key step in the sequence involves the elimination of water, which may serve to solubilize excess $NaHCO_{3(s)}$.

CONCLUSIONS

In summary, two crystal forms of ZnS were synthesized and evaluated for their photochemical properties. No significant differences were found between the synthesized particles with respect to absorption, location of CBM and VBM and band gap, yet photoreduction experiments demonstrated large differences in productivity. As hypothesized, the largest sized

DOI: 10.1021/acsami.5b06054
ACS Appl. Mater. Interfaces 2015, 7, 24543−24549

catalyst, mP-Sphal, demonstrated the lowest performance. The wurtzite crystal form showed the highest AQE of 0.9% when using IPA as the whole scavenger. The AQE increased to 3.2% when the electron donor was changed to glycerol. Given the large gain in productivity and the potential renewable source, glycerol is a preferable positive hole scavenger compared to other petroleum-derived candidates. Additionally, our results illustrate that ZnS crystal isoform clearly plays a role in the photocatalyzed reduction of bicarbonate to formate. The surface chemistry of specific crystal facets plays a role in determining the productivity of the catalyst. At this preliminary stage, our investigations do not distinguish between catalytic sites; further research is warranted. Studies by Rubasinghege et al. show a strong correlation between which crystal faces are solvent exposed and the reactivity of the catalyst.[43,44] Although these photocatalyzed results were dependent on AM 0 solar simulation conditions, their importance lies in identifying wurtzite as the more effective crystal. Moreover, applications involving carbon dioxide management via conversion to formate is relevant toward chemical conversion to electricity from fuel cells during manned spaceflight.[45,46] We are currently expanding the scope of this project to increase the absorption of the optical spectrum beyond the shortwave region of 350 nm by exploring photosensitized ZnS.

■ ASSOCIATED CONTENT

Supporting Information

The Supporting Information is available free of charge on the ACS Publications website at DOI: 10.1021/acsami.5b06054.

DLS size distribution plot, XRD spectra, cyclic voltammetry data, standard curves for formic acid analysis (PDF).

■ AUTHOR INFORMATION

Corresponding Author

*Michael D. Heagy. E-mail: mheagy@nmt.edu.

Funding

NSF award #IIA-1301346

Notes

The authors declare no competing financial interest.

■ ACKNOWLEDGMENTS

We thank Dr. Vigil Leuth for his help in running XRD analysis, Munawar Khalil for his expertise obtaining the surface area measurements, Dr. Michael Pullin and Dr. Asitha Cooray for their help developing the IC methods, Michael Malett for his help with cyclic voltammetry, and Dr. Matrin Kirk and Ben Stein for their help obtaining the DRS data. Funding for this project was provided by New Mexico EPSCoR.

■ DEDICATION

The authors wish to dedicate this article to Prof. George A. Olah on the occasion of his 88th birthday.

■ REFERENCES

(1) Olah, G. A.; Geoppert, A.; Prakash, G. K. *Beyond Oil and Gas: The Methanol Economy*; Wiley-VCH, Hoboken, NJ, 2009.

(2) Barton, E.; Rampulla, D.; Bocarsly, A. Selective Solar-Driven Reduction of CO_2 to Methanol Using a Catalyzed p-GaP Based Photoelectrochemical Cell. *J. Am. Chem. Soc.* **2008**, *130*, 6342−6344.

(3) Yuan, L.; Xu, Y.-J. Photocatalytic Conversion of CO_2 into Value-Added and Renewable Fuels. *Appl. Surf. Sci.* **2015**, *342*, 154−167.

(4) Indrakanti, V.; Kubicki, J.; Schobert, H. Photoinduced Activation of CO_2 on Ti-based Heterogeneous Catalysts: Current State, Chemical Physics-based Insights and Outlook. *Energy Environ. Sci.* **2009**, *2*, 745−758.

(5) Woolerton, T. W.; Sheard, S.; Reisner, E.; Pierce, E.; Ragsdale, S. W.; Armstrong, F. CO_2 Photoreduction at Enzyme-modified Metal Oxide Nanoparticles. *J. Am. Chem. Soc.* **2010**, *132*, 2132−2133.

(6) Jiang, Z.; Xiao, T.; Kuznetsov, V. L.; Edwards, P. Turning Carbon Dioxide into Fuel. *Philos. Trans. R. Soc., A* **2010**, *368*, 3343−3364.

(7) Sato, S.; Arai, T.; Morikawa, T.; Uemura, K. J.; Suzuki, T. M.; Tanaka, H.; Kajino, T. Selective CO_2 Conversion to Formate Conjugated with H_2O Oxidation Utilizing Semiconductor/Complex Hybrid Photocatalysts. *J. Am. Chem. Soc.* **2011**, *133*, 15240−15243.

(8) Cole, E.; Lakkaraju, P. S.; Rampulla, D. M.; Morris, A. J.; Abelev, A.; Bocarsly, A. B. Using a One-Electron Shuttle for the Multielectron Reduction of CO_2 to Methanol: Kinetic, Mechanistic, and Structural Insights. *J. Am. Chem. Soc.* **2010**, *132*, 11539−11551.

(9) Chaudhary, Y.; Woolerton, T. W.; Allen, C. S.; Warner, J. H.; Pierce, H.; Ragsdale, S. W.; Armstrong, F. A. Visible Light Driven CO_2 Reduction by Enzyme Coupled CdS Nanocrystals. *Chem. Commun.* **2012**, *48*, 58−60.

(10) Hussain, M.; Akhter, P.; Saracco, G.; Russo, N. Nanostructured TiO_2/KIT-6 Catalysts for Improved Photocatalytic Reduction of CO_2 to Tunable Energy Products. *Appl. Catal., B* **2015**, *170−171*, 53−65.

(11) Kuramochi, Y.; Itabashi, J.; Fukaya, K.; Enomoto, A.; Yoshida, M.; Ishida, H. Unexpected Effect of Catalyst Concentration on Photochemical CO_2 Reduction by trans(Cl)-Ru(byp) $(CO)_2(Cl)_2$: New Mechanistic Insight into the CO/$HCOO^-$. *Chem. Sci.* **2015**, *6*, 3063−3074.

(12) Habisreutinger, S.; Schmidt-Mende, L.; Stolarczyk. Photocatalytic Reduction of CO_2 on TiO_2 and Other Semiconductors J. *Angew. Chem., Int. Ed.* **2013**, *52*, 7372−7408.

(13) Kuwabata, S.; Nishida, K.; Tsuda, R.; Inoue, H.; Yoneyama, H. Photochemical Reduction of Carbon Dioxide to Methanol Using ZnS Microcrystallite as a Photocatalyst in the Presence of Methanol Dehydrogenase. *J. Electrochem. Soc.* **1994**, *141*, 1498−1503.

(14) Stalder, C.; Chao, S.; Wrighton, M. Electrochemical Reduction of Aqueous Bicarbonate to Formate with High Current Efficiency Near the Thermodynmic Potential at Chemically Derivitized Electrodes. *J. Am. Chem. Soc.* **1984**, *106*, 3673−3675.

(15) Zhang, X.; Martin, S. T.; Friend, C. M.; Schoonen, M. A. A.; Holland, H. D. Mineral-Assisted Pathways in Prebiotic Synthesis: Photoelectrochemical Reduction of Carbon(+IV) by Manganese Sulfide. *J. Am. Chem. Soc.* **2004**, *126*, 11247−11253.

(16) Irvine, J.; Eggins, B. Grimshaw, Solar Energy Fixation of Carbon Dioxide via Cadmium Sulphide and Other Semiconductor Photocatalysts. *Sol. Energy* **1990**, *45*, 27−33.

(17) Johne, P.; Kisch, H. Photoreduction of Carbon Dioxide Catalysed by Free and Supported Zinc and Cadmium Sulphide Powders. *J. Photochem. Photobiol., A* **1997**, *111*, 223−228.

(18) Dimitrijevic, N. D.; Shkrob, I. A.; Gosztola, D. J.; Rajh, T. Dynamics of Interfacial Charge Transfer to Formic Acid, Formaldehyde, and Methanol on the Surface of TiO_2 Nanoparticles and Its Role in Methane Production. *J. Phys. Chem. C* **2012**, *116*, 878−885.

(19) Electrochemical oxidation values for glycerol and ehtylene glycol obtained from: Falase, A.; Main, M.; Garcia, K.; Serov, A.; Lau, C.; Atanassov, P. Electrooxidation of Ethylene Glycol and Glycerol by Platinum-Bsed Binary and Ternary Nanoscrtuctured Catalysts. *Electrochim. Acta* **2012**, *66*, 295−301. Electrochemical oxidation value for propan-2-ol obtained experimentally from the Supporting Information.

(20) Christoph, R.; Schmidt, B.; Steinberner, U.; Dilla, W.; Karinen, R. Glycerol. In *Ullmann's Encyclopedia of Industrial Chemistry*; Wiley-VCH: Hoboken, NJ, 2000.

(21) John, R.; Florence, S. Optical, Structural and Morphological Studies of Bean-like ZnS Nanostructures by Aqueous Chemical Method. *Chalcogenide Lett.* **2010**, *7*, 269−273.

(22) She, Y. Y.; Yang, J.; Qiu, K. Synthesis of ZnS Nanoparticles by Solid-Liquid Chemical Reaction of ZnO and Na_2S Under Ultrasonic. *Trans. Nonferrous Met. Soc. China* **2010**, *20*, s211−s215.

DOI: 10.1021/acsami.5b06054
ACS Appl. Mater. Interfaces 2015, 7, 24543−24549

(23) Zhang, Y. H.; Zhang, N.; Tang, Z. R.; Xu, Y. J. Graphene Transforms Wide Band Gap ZnS to a Vizible Light Photocatalyst. The New Role of Graphene as a Macromolecular Photosensitizer. *ACS Nano* **2012**, *6*, 9777−9789.
(24) Fang, Y. M.; Sun, J. J.; Wu, A. H.; Su, X. L.; Chen, G. N. Catalytic Electrogenerated Chemiluminescence and Nitrate Reduction at CdS Nanotubes Modified Glassy Carbon Electrode. *Langmuir* **2009**, *25*, 555−560.
(25) Ohtani, B. Photocatalysis A to Z—What We Know and What We Do Not Know in a Scientific Sense. *J. Photochem. Photobiol., C* **2010**, *11*, 157−178.
(26) Quigg, A.; Chin, W. C.; Chen, C. S.; Zhang, S. J.; Jiang, Y. L.; Miao, A.; Schwehr, K. A.; Xu, C.; Santschi, P. Direct and Indirect Toxic Effects of Engineered Nanoparticles on Algae: Role of Natural Organic Matter. *ACS Sustainable Chem. Eng.* **2013**, *1*, 686−702.
(27) Soloviev, N. V.; Eichofer, A.; Fenske, D.; Banin, U. Molecular Limit of a Bulk Semiconductor: Size Dependence of the "Band Gap" in CdSe Cluster Molecules. *J. Am. Chem. Soc.* **2000**, *122*, 2673−2674.
(28) Strehlow, W. H.; Cook, E. L. Compilation of Energy Band Gaps in Elemental and Binary Compound Semiconductors and Insulators. *J. Phys. Chem. Ref. Data* **1973**, *2*, 163−199.
(29) Calculated from the molar production values. Kaneco, S.; Shimizu, Y.; Ohta, K.; Mizuno, T. Photocatalytic Reduction of High Pressure Carbon Dioxide using TiO_2 Powders with a Positive Hole Scavenger. *J. Photochem. Photobiol., A* **1998**, *115*, 223−226.
(30) Stalder, C.; Chao, S.; Summers, D. P.; Wrighton, M. S. Supported Palladium Catalysts for the Reduction of Sodium Bicarbonate to Sodium Formate in Aqueous Solution at Room Temperature and One Atmosphere of Hydrogen. *J. Am. Chem. Soc.* **1983**, *105*, 6318−6320.
(31) Willner, I.; Mandler, D. Characterization of Pd-β-Cyclodextrin Colloids as Catalysts in the Photosensitized Reduction of Bicarbonate to Formate. *J. Am. Chem. Soc.* **1989**, *111*, 1330−1336.
(32) Kisch, H.; Lutz, P. Photoreduction of Bicarbonate Catalyzed by Supported Cadmium Sulfide. *Photochem. Photobiol. Sci.* **2002**, *1*, 240−245.
(33) Mandler, D.; Willner, I. Effective Photoreduction of CO_2/HCO_3^- to Formate Using Visible Light. *J. Am. Chem. Soc.* **1987**, *109*, 7884−7885.
(34) Strumm, W.; Morgan, J. J. *Aquatic Chemistry*, 3rd ed.; Wiley Interscience: New York, 1996.
(35) Tanaka, K.; Capule, M.; Hisanaga, T. Effect of Crystallinity of TiO_2 on Its Photocatalytic Action. *Chem. Phys. Lett.* **1991**, *187*, 73−76.
(36) Linsebigler, A. L.; Lu, G.; Yates, J. T. Photocatalysis on TiO_2 Surfaces: Principles, Mechanisms, and Selected Results. *Chem. Rev.* **1995**, *95*, 735−758.
(37) Ohno, T.; Tokieda, K.; Higashida, S.; Matsumura, M. Synergism Between Rutile and Anatase TiO_2 Particles in Photocatalytic Oxidation of Naphthalene. *Appl. Catal., A* **2003**, *244*, 383−391.
(38) Hong, Y.; Lin, Z.; Huang, J.; Wang, Y.; Huang, F. Study on the Influence of Lattice Integrity and Phase Composition to the Photocatalytic Efficiency of ZnS Material. *Nanoscale* **2011**, *3*, 1512−1515.
(39) Hong, Y.; Zhang, J.; Wang, X.; Wang, Y.; Lin, Z.; Yu, J.; Huang, F. Influence of Lattice Integrity and Phase Composition on the Photocatalytic Hydrogen Production Efficiency of ZnS Nanomaterials. *Nanoscale* **2012**, *4*, 2859−2862.
(40) Wang, Y.; Huang, F.; Pan, D.; Li, B.; Chen, D.; Lin, W.; Chen, X.; Li, R.; Lin, Z. Ultraviolet-Light-Induced Bactericidal Mechanism on ZnO Single Crystals. *Chem. Commun.* **2009**, 6783−6785.
(41) Di Valentin, C.; Fittipaldi, D. Hole Scavenging by Organic Adsorbates on the TiO_2 Surface: A DFT Model Study. *J. Phys. Chem. Lett.* **2013**, *4*, 1901−1906.
(42) Williams, G.; Kamat, P. Graphene-Semiconductor Nanocomposites: Excited-State Interactions between ZnO Nanoparticles and Graphene Oxide. *Langmuir* **2009**, *25*, 13869−13873.
(43) Rubasinghege, G.; Lentz, R.; Scherer, M. M.; Grassian, V. H. Simulated Atmospheric Processing of Iron Oxyhydroxide Minerals at Low pH: Roles of Particle Size and Acid Anion in Iron Dissolution. *Proc. Natl. Acad. Sci. U. S. A.* **2010**, *107*, 6628−6633.
(44) Wijenayaka, L. A.; Rubasinghege, G.; Baltrusaitis, J.; Grassian, V. H. Surface Chemistry of α-FeOOH Nanorods with Gas-Phase Nitric Acid and Water Vapor: Insights into the Role of Particle Size, Surface Structure, and Surface Hydroxyl Groups in the Adsorption and Reactivity of α-FeOOH with Atmospheric Gases. *J. Phys. Chem. C* **2012**, *116*, 12566−12577.
(45) Mattox, E. M.; Knox, J. C.; Bardot, D. M. Carbon Dioxide Removal System for Closed Loop Atmosphere Revitalization, Candidate Sorbents Screening and Test Results. *Acta Astronaut.* **2013**, *86*, 39−46.
(46) Jiang, J. H.; Wieckowski, A. Prospective Direct Formate Fuel Cell. *Electrochem. Commun.* **2012**, *18*, 41−43.

DOI: 10.1021/acsami.5b06054
ACS Appl. Mater. Interfaces 2015, 7, 24543−24549

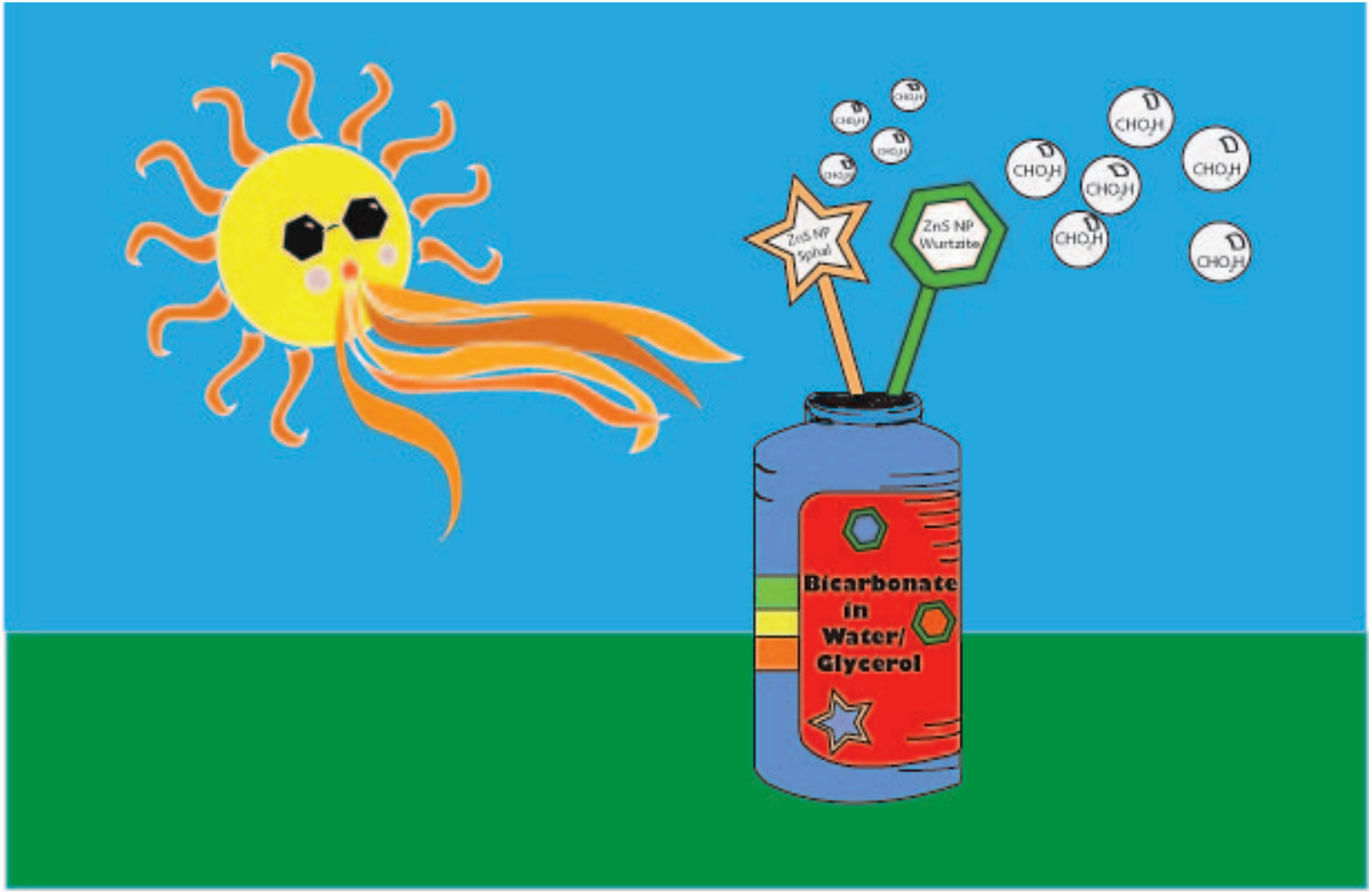
ZnS NP Sphal
ZnS NP Wurtzite
CHO2H
Bicarbonate in Water/ Glycerol